

# Nuclear constraints on the momenta of inertia of neutron stars

Aaron Worley, Plamen G. Krastev and Bao-An Li

*Department of Physics, Texas A&M University-Commerce, Commerce, TX 75429, U.S.A.*

aworley@leo.tamu-commerce.edu, Plamen\_Krastev@tamu-commerce.edu,  
Bao-An\_Li@tamu-commerce.edu

## ABSTRACT

Properties and structure of neutron stars are determined by the equation of state (EOS) of neutron-rich stellar matter. While the collective flow and particle production in relativistic heavy-ion collisions have constrained tightly the EOS of symmetric nuclear matter up to about five times the normal nuclear matter density, the more recent experimental data on isospin-diffusion and isoscaling in heavy-ion collisions at intermediate energies have constrained considerably the density dependence of the nuclear symmetry energy at subsaturation densities. Although there are still many uncertainties and challenges to pin down completely the EOS of neutron-rich nuclear matter, the heavy-ion reaction experiments in terrestrial laboratories have limited the EOS of neutron-rich nuclear matter in a range much narrower than that spanned by various EOSs currently used in astrophysical studies in the literature. These nuclear physics constraints could thus provide more reliable information about properties of neutron stars. Within well established formalisms using the nuclear constrained EOSs we study the momenta of inertia of neutron stars. We put the special emphasis on the component A of the extremely relativistic double neutron star system PSR J0737-3039. Its moment of inertia is found to be between 1.30 and 1.63 ( $\times 10^{45} g cm^2$ ). Moreover, the transition density at the crust-core boundary is shown to be in the narrow range of  $\rho_t = [0.091 - 0.093](fm^{-3})$ .

*Subject headings:* dense matter — equation of state — stars: neutron — stars: rotation

## 1. Introduction

Neutron stars exhibit a large array of extreme characteristics. Their properties and structure are determined by the equation of state (EOS) of neutron-rich stellar matter at densities up to an order of magnitude higher than those found in ordinary nuclei, see, e.g. Weber

(1999) and Lattimer & Prakash (2004). Therefore, the detailed knowledge about the EOS of neutron-rich nuclear matter over a wide range of densities is necessary for the study of neutron stars. For isospin asymmetric nuclear matter, various theoretical studies have shown that the energy per nucleon can be well approximated by

$$E(\rho, \delta) = E(\rho, \delta = 0) + E_{\text{sym}}(\rho)\delta^2 + O(\delta^4), \quad (1)$$

in terms of the baryon density  $\rho = \rho_n + \rho_p$ , the isospin asymmetry  $\delta = (\rho_n - \rho_p)/(\rho_n + \rho_p)$ , the energy per nucleon in symmetric nuclear matter  $E(\rho, \delta = 0)$ , and the bulk nuclear symmetry energy  $E_{\text{sym}}(\rho)$ . Here we report the results of a study on the moment of inertia and the core-crust transition density of neutron stars within well established formalisms in the literature using several EOSs constrained by the latest terrestrial heavy-ion reaction experiments.

Presently, besides the possibilities of phase transitions into various non-nucleonic states the behavior of nuclear matter under extreme densities, pressures and/or isospin-asymmetry is still highly uncertain and relies upon, often, rather controversial theoretical predictions. This circumstance introduces corresponding uncertainties in the EOS of neutron-rich nuclear matter and thus limits our ability to understand many key issues in astrophysics. While astrophysical observations can also limit the EOS of neutron-rich nuclear matter, terrestrial laboratories experiments provide complementary information and have their unique advantages. In this regard, it is especially interesting to mention that the collective flow and particle production in relativistic heavy-ion collisions have constrained the EOS of symmetric nuclear matter  $E(\rho, \delta = 0)$  up to about five times the normal nuclear matter density to a narrow range (Danielewicz, Lacey, & Lynch 2002). However, there are still many challenges and uncertainties in pinning down precisely the EOS of neutron-rich nuclear matter. One of the major remaining uncertainties is the density dependence of the nuclear symmetry energy  $E_{\text{sym}}(\rho)$ , see e.g. Refs. (Lattimer & Prakash 2004; Steiner et al. 2005; Chen et al. 2007) for recent reviews. To constrain the density dependence of the symmetry energy, many terrestrial nuclear experiments have been carried out recently or planned. Depending on the techniques used, some experiments are more useful for exploring the symmetry energy at low densities while others are more effective at high densities. For instance, heavy-ion reactions, especially those involving radioactive beams, provide a unique means to probe the  $E_{\text{sym}}(\rho)$  over a broad density range (Li et al. 1998; Li & Udo Schroeder 2001; Baran et al. 2005; Chen et al. 2007). In fact, some significant progress has been made very recently by studying the isospin diffusion (Shi & Danielewicz 2003; Tsang et al. 2004; Chen et al. 2005; Li & Chen 2005) and isoscaling (Tsang et al. 2001; Shetty, Yennello & Souliotis 2007) in heavy-ion reactions at intermediate energies. The analysis of these phenomena based on transport theories of heavy-ion reactions and thermodynamical models of nuclear multifragmentation has limited the  $E_{\text{sym}}(\rho)$  in a range much narrower than that spanned by various forms of the  $E_{\text{sym}}(\rho)$  currently used in astrophysical studies in the literature. Moreover,

the lower bound of the  $E_{sym}(\rho)$  extracted from the heavy-ion reactions is consistent with the RMF prediction using the FSUGold interaction that can reproduce not only saturation properties of nuclear matter but also structure properties and giant resonances of many finite nuclei (Piekraewicz 2007).

It is also well known that the sizes of neutron skins in heavy nuclei are sensitive to the symmetry energy at subsaturation densities, see, e.g., Refs. (Brown 2000; Horowitz & Piekarewicz 2001, 2002; Dieperink et al. 2003; Furnstahl 2002; Steiner et al. 2005; Todd-Rutel & Piekarewicz 2005; Steiner & Li 2005; Chen et al. 2005). However, available data of neutron-skin thickness obtained using hadronic probes are not accurate enough to constrain significantly the symmetry energy. Interestingly, the parity radius experiment (PREX) at the Jefferson Laboratory aiming to measure the neutron radius in  $^{208}\text{Pb}$  via parity violating electron scattering (Jefferson Laboratory Experiment E-00-003) (Horowitz et al. 2001) hopefully will provide much more precise data and thus constrain the symmetry energy at low densities more tightly in the near future. On the other hand, at supranormal densities, a number of potential probes of the symmetry energy have been proposed (Li et al. 1997; Li 2000, 2002; Li et al. 1998; Chen et al. 2007). Moreover, several experiments to probe the high density behavior of the symmetry energy with high energy radioactive beams have been planned at the CSR/Lanzhou, FAIR/GSI, RIKEN and the NSCL/MSU.

While the EOS of neutron-rich nuclear matter has not been completely determined yet, it is still very interesting to examine astrophysical implications of the EOS constrained by the latest terrestrial laboratory experiments mentioned above. Global properties of spherically symmetric static (non-rotating) neutron stars have been studied extensively over many years, for recent reviews, see, e.g., Refs. (Lattimer & Prakash 2000, 2004; Prakash et al. 2001; Yakovlev & Pethick 2004; Heiselberg & Pandharipande 2000; Heiselberg & Hjorth-Jensen 2000; Steiner et al. 2005). However, properties of (rapidly) rotating neutron stars have been investigated to lesser extent. Models of (rapidly) rotating neutron stars have been constructed only by several research groups with various degree of approximation (Hartle 1967; Hartle & Thorne 1968; Friedman et al. 1986; Bombaci et al. 2000; Lattimer et al. 1990; Komatsu et al. 1989; Cook et al. 1994; Stergioulas & Friedman 1995, 1998; Bonazzola et al. 1993, 1998; Weber 1999; Ansorg et al. 2002) (see Stergioulas (2003) for a review). In a recent work (Krastev et al. 2008) we have reported predictions on the gravitational masses, radii, maximal rotational (Kepler) frequencies, and thermal properties of (rapidly) rotating neutron stars. In this work, using the nuclear constrained EOSs we calculate the momenta of inertia for both spherically-symmetric (static) and (rapidly) rotating neutron stars using well established formalisms in the literature. Such studies are important and timely as they are related to the astrophysical observations in the near future. In particular, the moment of inertia of pulsar  $A$  in the extremely relativistic neutron star binary PSR J0737-3039

(Burgay et al. 2003) may be determined in a few years through detailed measurements of the periastron advance (Bejger et al. 2005).

## 2. The equation of state of neutron-rich nuclear matter constrained by recent data from terrestrial heavy-ion reactions

In this section, we first outline the theoretical tools one uses to extract information about the EOS of neutron-rich nuclear matter from heavy-ion collisions. We put the special emphasis on exploring the density-dependence of the symmetry energy as the study on the EOS of symmetric nuclear matter with heavy-ion reactions is better known to the astrophysical community and it has been extensively reviewed, see e.g., Refs. (Danielewicz, Lacey, & Lynch 2002; Steiner et al. 2005; Lattimer & Prakash 2007) for recent reviews. We will then summarize the latest constraints on the density dependence of the symmetry energy extracted from studying isospin diffusion and isoscaling in heavy-ion reactions at intermediate energies. Finally, we address the question of what kind of isospin-asymmetry, especially for dense matter, can be reached in heavy-ion reactions.

Heavy-ion reactions are a unique means to create in terrestrial laboratories dense nuclear matter similar to those found in the core of neutron stars. Depending on the beam energy, impact parameter and the reaction system, various hadrons and/or partons may be created during the reaction. To extract information about the EOS of dense matter from heavy-ion reactions requires careful modelling of the reaction dynamics and selection of sensitive observables. Among the available tools, computer simulations based on the Boltzmann-Uehling-Uhlenbeck (BUU) transport theory have been very useful, see, e.g., Refs. (Bertsch & Das Gupta 1988; Danielewicz, Lacey, & Lynch 2002) for reviews. The evolution of the phase space distribution function  $f_i(\vec{r}, \vec{p}, t)$  of nucleon  $i$  is governed by both the mean field potential  $U$  and the collision integral  $I_{collision}$  via the BUU equation

$$\frac{\partial f_i}{\partial t} + \vec{\nabla}_p U \cdot \vec{\nabla}_r f_i - \vec{\nabla}_r U \cdot \vec{\nabla}_p f_i = I_{collision}. \quad (2)$$

Normally, effects of the collision integral  $I_{collision}$  via both elastic and inelastic channels including particle productions, such as pions, are modelled via Monte Carlo sampling using either free-space experimental data or calculated in-medium cross sections for the elementary hadron-hadron scatterings (Bertsch & Das Gupta 1988). Information about the EOS is obtained from the underlying mean-field potential  $U$  which is an input to the transport model. By comparing experimental data on some carefully selected observables with transport model predictions using different mean-field potentials corresponding to various EOSs, one can then constrain the corresponding EOS. The specific constraints on the density de-

pendence of the nuclear symmetry energy that we are using in this work were obtained by analyzing the isospin diffusion data (Tsang et al. 2004) within the IBUU04 version of an isospin and momentum dependent transport model (Li et al. 2004). In this model, an isospin and momentum-dependent interaction (MDI) (Das et al. 2003) is used. With this interaction, the potential energy density  $V(\rho, T, \delta)$  at total density  $\rho$ , temperature  $T$  and isospin asymmetry  $\delta$  is

$$V(\rho, T, \delta) = \frac{A_u \rho_n \rho_p}{\rho_0} + \frac{A_l}{2\rho_0}(\rho_n^2 + \rho_p^2) + \frac{B}{\sigma + 1} \frac{\rho^{\sigma+1}}{\rho_0^\sigma} (1 - x\delta^2) + \sum_{\tau, \tau'} \frac{C_{\tau, \tau'}}{\rho_0} \int \int d^3 p d^3 p' \frac{f_\tau(\vec{r}, \vec{p}) f_{\tau'}(\vec{r}, \vec{p}')}{1 + (\vec{p} - \vec{p}')^2 / \Lambda^2} \quad (3)$$

In the mean field approximation, Eq. (3) leads to the following single particle potential for a nucleon with momentum  $\vec{p}$  and isospin  $\tau$

$$U_\tau(\rho, T, \delta, \vec{p}, x) = A_u(x) \frac{\rho_{-\tau}}{\rho_0} + A_l(x) \frac{\rho_\tau}{\rho_0} + B \left( \frac{\rho}{\rho_0} \right)^\sigma (1 - x\delta^2) - 8\tau x \frac{B}{\sigma + 1} \frac{\rho^{\sigma-1}}{\rho_0^\sigma} \delta \rho_{-\tau} + \sum_{t=\tau, -\tau} \frac{2C_{\tau, t}}{\rho_0} \int d^3 \vec{p}' \frac{f_t(\vec{r}, \vec{p}')}{1 + (\vec{p} - \vec{p}')^2 / \Lambda^2}, \quad (4)$$

where  $\tau = 1/2$  ( $-1/2$ ) for neutrons (protons),  $x$ ,  $A_u(x)$ ,  $A_l(x)$ ,  $B$ ,  $C_{\tau, \tau}$ ,  $C_{\tau, -\tau}$ ,  $\sigma$ , and  $\Lambda$  are all parameters given in Ref. (Das et al. 2003). The last two terms in Eq. (4) contain the momentum dependence of the single-particle potential, including that of the symmetry potential if one allows for different interaction strength parameters  $C_{\tau, -\tau}$  and  $C_{\tau, \tau}$  for a nucleon of isospin  $\tau$  interacting, respectively, with unlike and like nucleons in the background fields. It is worth mentioning that the nucleon isoscalar potential estimated from  $U_{isoscalar} \approx (U_n + U_p)/2$  agrees with the prediction of variational many-body calculations for symmetric nuclear matter (Wiringa 1988) in a broad density and momentum range (Li et al. 2004). Moreover, the EOS of symmetric nuclear matter for this interaction is consistent with that extracted from the available data on collective flow and particle production in relativistic heavy-ion collisions up to five times the normal nuclear matter (Danielewicz, Lacey, & Lynch 2002; Krastev et al. 2008). On the other hand, the corresponding isovector (symmetry) potential can be estimated from  $U_{sym} \approx (U_n - U_p)/2\delta$ . At normal nuclear matter density, the MDI symmetry potential agrees very well with the Lane potential extracted from nucleon-nucleus and (n,p) charge exchange reactions available for nucleon kinetic energies up to about 100 MeV (Li et al. 2004). At abnormal densities and higher nucleon energies, however, there is no experimental constrain on the symmetry potential available at present.

The different  $x$  values in the MDI interaction are introduced to vary the density dependence of the nuclear symmetry energy while keeping other properties of the nuclear equation

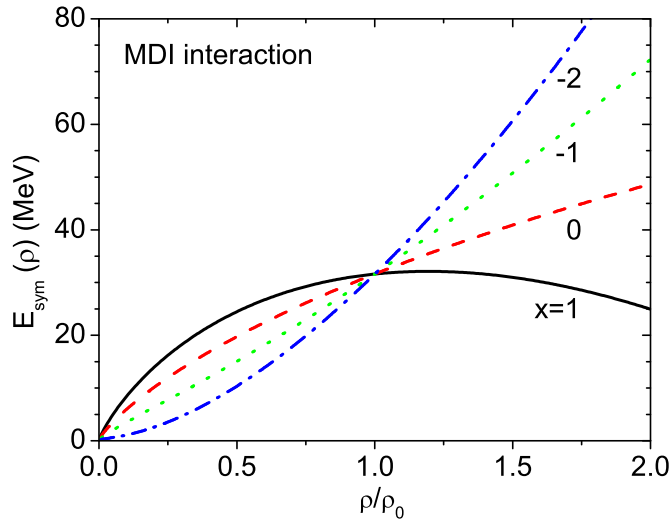


Fig. 1.— The density dependence of the nuclear symmetry energy for different values of the parameter  $x$  in the MDI interaction. Taken from (Li et al. 2005).

of state fixed. Specifically, choosing the incompressibility  $K_0$  of cold symmetric nuclear matter at saturation density  $\rho_0$  to be 211 MeV leads to the dependence of the parameters  $A_u$  and  $A_l$  on the  $x$  parameter according to

$$A_u(x) = -95.98 - x \frac{2B}{\sigma + 1}, \quad A_l(x) = -120.57 + x \frac{2B}{\sigma + 1}, \quad (5)$$

with  $B = 106.35$  MeV.

With the potential contribution in Eq. 3 and the well-known contribution from nucleon kinetic energies in the Fermi gas model, the EOS and the symmetry energy at zero temperature can be easily obtained. As shown in Fig. 1, adjusting the parameter  $x$  leads to a broad range of the density dependence of the nuclear symmetry energy, similar to those predicted by various microscopic and/or phenomenological many-body theories. As demonstrated by Li & Chen (2005) and Li & Steiner (2006), only equations of state with  $x$  between -1 and 0 have symmetry energies in the sub-saturation density region consistent with the isospin diffusion data and the available measurements of the skin thickness of  $^{208}\text{Pb}$  using hadronic probes. Moreover, it is interesting to note that the symmetry energy extracted very recently from the isoscaling analyses of heavy-ion reactions is consistent with the MDI calculation using  $x = 0$  (Shetty, Yennello & Souliotis 2007). The  $E_{sym}(\rho)$  with  $x = 0$  is also consistent with the RMF prediction using the FSUGold interaction (Piekraewicz 2007). We thus consider only the two limiting cases with  $x = 0$  and  $x = -1$  as boundaries of the symmetry energy consistent with the available terrestrial nuclear laboratory data.

Table 1: The parameters  $F$  (MeV),  $G$ ,  $K_{sym}$  (MeV),  $L$  (MeV), and  $K_{asy}$  (MeV) for different values of  $x$ . Taken from (Chen et al. 2005).

$x$	$F$	$G$	$K_{sym}$	$L$	$K_{asy}$
1	107.232	1.246	-270.4	16.4	-368.8
0	129.981	1.059	-88.6	62.1	-461.2
-1	3.673	1.569	94.1	107.4	-550.3
-2	-38.395	1.416	276.3	153.0	-641.7

To ease comparisons with other models in the literature, it is useful to parameterize the  $E_{sym}(\rho)$  from the MDI interaction and list its characteristics. Within phenomenological models it is customary to separate the symmetry energy into the kinetic and potential parts, see, e.g. (Prakash et al. 1988),

$$E_{sym}(\rho) = (2^{2/3} - 1) \frac{3}{5} E_F^0 (\rho/\rho_0)^{2/3} + E_{sym}^{\text{pot}}(\rho). \quad (6)$$

With the MDI interaction, the potential part of the nuclear symmetry energy can be well parameterized by

$$E_{sym}^{\text{pot}}(\rho) = F(x)\rho/\rho_0 + (18.6 - F(x))(\rho/\rho_0)^{G(x)}, \quad (7)$$

with  $F(x)$  and  $G(x)$  given in Table 1 for  $x = 1, 0, -1$  and  $-2$ . The MDI parameterizations for the  $E_{sym}^{\text{pot}}(\rho)$  is similar but significantly different from those used by Prakash et al. (1988). Also shown in Table 1 are other characteristics of the symmetry energy, including its slope parameter  $L$  and curvature parameter  $K_{sym}$  at  $\rho_0$ , as well as the isospin-dependent part  $K_{asy}$  of the isobaric incompressibility of asymmetric nuclear matter (Chen et al. 2005). The symmetry energy in the subsaturation density region with  $x=0$  and  $-1$  can be roughly approximated by  $E_{sym}(\rho) \approx 31.6(\rho/\rho_0)^{0.69}$  and  $E_{sym}(\rho) \approx 31.6(\rho/\rho_0)^{1.05}$ , respectively.

The MDI EOS has been recently applied to constrain the mass-radius correlations of both static and rapidly rotating neutron stars (Li & Steiner 2006; Krastev et al. 2008). In addition, it has been also used to constrain a possible time variation of the gravitational constant  $G$  (Krastev & Li 2007) via the gravitochemical heating formalism developed by Jofre et al. (2006). For comparisons, in this work we apply also EOSs from variational calculations with the  $A18+\delta v+UIX^*$  interaction (APR) Akmal et al. (1998), and recent Dirac-Brueckner-Hartree-Fock (DBHF) calculations (Alonso & Sammarruca 2003; Krastev & Sammarruca 2006) (DBHF+Bonn B) with Bonn B One-Boson-Exchange (OBE) potential (Machleidt 1989). Below the baryon density of approximately  $0.07 fm^{-3}$  the equations of state are supplemented by a crustal EOS, which is more suitable for the low density regime. Namely,

Table 2: Saturation properties of the nuclear EOSs (for symmetric nuclear matter) employed in this work. Taken from (Krastev et al. 2008).

EOS	$\rho_0(fm^{-3})$	$E_s(MeV)$	$\kappa(MeV)$	$e_{sym}(\rho_0)(MeV)$	$m^*(\rho_0)/m$
MDI(x=0)	0.160	-16.08	211.00	31.62	0.67
MDI(x=-1)	0.160	-16.08	211.00	31.62	0.67
APR	0.160	-16.00	266.00	32.60	0.70
DBHF+Bonn B	0.185	-16.14	259.04	33.71	0.65

The first column identifies the equation of state. The remaining columns exhibit the following quantities at the nuclear saturation density: saturation (baryon) density; energy-per-particle; compression modulus; symmetry energy; nucleon effective mass to *average* nucleon mass ratio (with  $m = 938.926 MeV c^{-2}$ ).

we apply the EOS by Pethick, Ravenhall & Lorenz (1995) for the inner crust and the one by Haensel & Pichon (1994) for the outer crust. At the highest densities we assume a continuous functional for the EOSs employed in this work. (See (Krastev & Sammarruca 2006) for a detailed description of the extrapolation procedure for the DBHF+Bonn B EOS.) The saturation properties of the nuclear equations of state used in this paper are summarized in Table 2.

What is the maximum isospin asymmetry reached, especially in the supra-normal density regions, in typical heavy-ion reactions? How does it depend on the symmetry energy? Do both the density and isospin asymmetry reached have to be high simultaneously in order to probe the symmetry energy at supra-normal densities with heavy-ion reactions? The answers to these questions are important for us to better understand the advantages and limitations of using heavy-ion reactions to probe the EOS of neutron-rich nuclear matter and properly evaluate their impacts on astrophysics.

To answer these questions we first show in Fig. 2 the central baryon density (upper window) and the average  $(n/p)_{\rho \geq \rho_0}$  ratio (lower window) of all regions with baryon densities *higher than*  $\rho_0$  in the reaction of  $^{132}Sn + ^{124}Sn$  at a beam energy of 400 MeV/nucleon and an impact parameter of 1 fm. It is seen that the maximum baryon density is about 2 times normal nuclear matter density. Moreover, the compression is rather insensitive to the symmetry energy because the latter is relatively small compared to the EOS of symmetric nuclear matter around this density. The high density phase lasts for about 15 fm/c from 5 to 20 fm/c for this reaction. It is interesting to see in the lower window that the isospin asymmetry of the high density region is quite sensitive to the density dependence of the symmetry energy used in the calculation. The soft (e.g.,  $x = 1$ ) symmetry energy

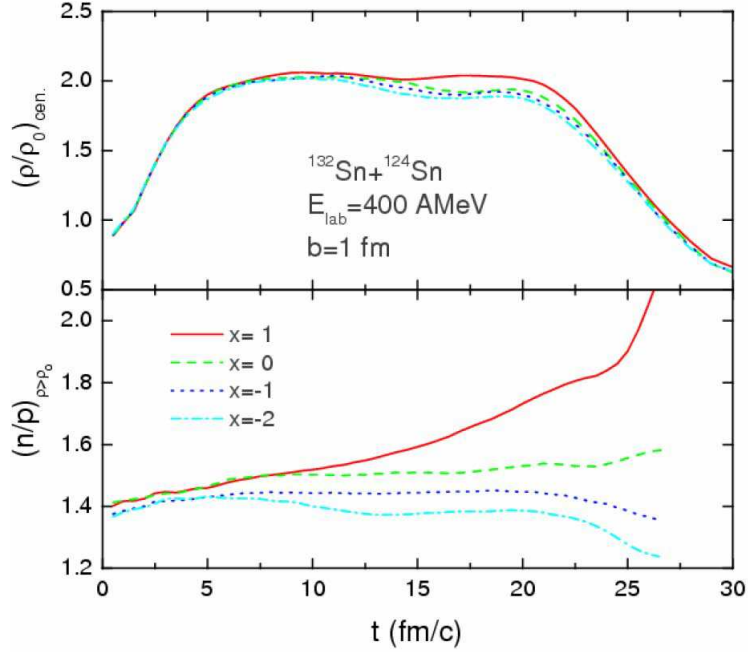


Fig. 2.— Central baryon density (upper panel) and isospin asymmetry (lower panel) of high density region in the reaction of  $^{132}\text{Sn} + ^{124}\text{Sn}$  at a beam energy of 400 MeV/nucleon and an impact parameter of 1 fm. Taken from Ref. (Li et al. 2005).

leads to a significantly higher value of  $(n/p)_{\rho \geq \rho_0}$  than the stiff one (e.g.,  $x = -2$ ). This is consistent with the well-known isospin fractionation phenomenon in asymmetric nuclear matter (Muller & Serot 1995; Li & Ko 1997). Because of the  $E_{sym}(\rho)\delta^2$  term in the EOS of asymmetric nuclear matter, it is energetically more favorable to have a higher isospin asymmetry  $\delta$  in the high density region with a softer symmetry energy functional  $E_{sym}(\rho)$ . In the supra-normal density region, as shown in Fig. 1, the symmetry energy changes from being soft to stiff when the parameter  $x$  varies from 1 to -2. Thus the value of  $(n/p)_{\rho \geq \rho_0}$  becomes lower as the parameter  $x$  changes from 1 to -2. It is worth mentioning that the initial value of the quantity  $(n/p)_{\rho \geq \rho_0}$  is about 1.4 which is less than the average n/p ratio of 1.56 of the reaction system. This is because of the neutron-skins of the colliding nuclei, especially that of the projectile  $^{132}\text{Sn}$ . In the neutron-rich nuclei, the n/p ratio on the low-density surface is much higher than that in their interior. Also because of the  $E_{sym}(\rho)\delta^2$  term in the EOS, the isospin-asymmetry in the low density region is much lower than the supra-normal density region as long as the symmetry increases with density. In fact, as shown in Fig. 2 of Ref. (Li & Steiner 2006), the isospin-asymmetry of the low density region can become much higher than the isospin asymmetry of the reaction system.

It is clearly seen that the dense region can become either neutron-richer or neutron-poorer with respect to the initial state depending on the symmetry energy functional  $E_{sym}(\rho)$  used. As long as the symmetry energy increases with the increasing density, the isospin asymmetry of the supra-normal density region is always lower than the isospin asymmetry of the reaction system. Thus, even with radioactive beams, the supra-normal density region can not be both dense and neutron-rich simultaneously, unlike the situation in the core of neutron stars, unless the symmetry energy starts decreasing at high densities. The high density behavior of the symmetry energy is probably among the most uncertain properties of dense matter as stressed by (Kutschera et al. 1993; Kutschera 2000). Indeed, some predictions show that the symmetry energy can decrease with increasing density above certain density and may even finally becomes negative. This extreme behavior was first predicted by some microscopic many-body theories, see e.g., Refs. (Pandharipande & Garde 1972; Wiringa 1988a; Krastev & Sammarruca 2006). It has also been shown that the symmetry energy can become negative at various high densities within the Hartree-Fock approach using the original Gogny force (Chabanat et al. 1997), the density-dependent M3Y interaction (Khoa et al. 1996; Basu et al. 2006) and about 2/3 of the 87 Skyrme interactions that have been widely used in the literature (Stone et al. 2003). The mechanism and physical meaning of a negative symmetry energy are still under debate and certainly deserve more studies.

Isospin effects in heavy-ion reactions are determined mainly by the  $E_{sym}(\rho)\delta^2$  term in the EOS. One expects a larger effect if the isospin-asymmetry is higher. Thus, ideally, one would like to have situations where both the density and isospin asymmetry are sufficiently high simultaneously as in the cores of neutron stars in order to observe the strongest effects due to the symmetry energy at supra-normal densities. However, since it is the product of the symmetry energy and the isospin-asymmetry that matters, one can still probe the symmetry energy at high densities where the isospin asymmetry is generally low with symmetry energy functionals that increase with density. Therefore, even if the high density region may not be as neutron-rich as in neutron stars, heavy-ion collisions can still be used to probe the symmetry energy at high densities useful for studying properties of neutron stars.

### 3. The moment of inertia of neutron stars

Employing the EOSs described briefly in Section 2, we compute the neutron star moment of inertia with the *RNS*<sup>1</sup> code developed and made available to the public by Nikolaos Stergioulas (Stergioulas & Friedman 1995). The code solves the hydrostatic and Einstein’s field equations for mass distributions rotating rigidly under the assumption of stationary and axial symmetry about the rotational axis, and reflectional symmetry about the equatorial plane. *RNS* calculates the angular momentum  $J$  as (Stergioulas 2003)

$$J = \int T^{\mu\nu} \xi_{(\phi)}^\nu dV, \quad (8)$$

where  $T^{\mu\nu}$  is the energy-momentum tensor of stellar matter

$$T^{\mu\nu} = (\epsilon + P)u^\mu u^\nu + P g^{\mu\nu}, \quad (9)$$

$\xi_{(\phi)}^\nu$  is the Killing vector in azimuthal direction reflecting axial symmetry, and  $dV = \sqrt{-g}d^3x$  is a proper 3-volume element ( $g \equiv \det(g_{\alpha\beta})$  is the determinant of the 3-metric). In Eq. (9)  $P$  is the pressure,  $\epsilon$  is the mass-energy density, and  $u^\mu$  is the unit time-like four-velocity satisfying  $u^\mu u_\mu = -1$ . For axial-symmetric stars it takes the form  $u^\mu = u^t(1, 0, 0, \Omega)$ , where  $\Omega$  is the star’s angular velocity. Under this condition Eq. (8) reduces to

$$J = \int (\epsilon + P)u^t(g_{\phi\phi}u^\phi + g_{\phi t}u^t)\sqrt{-g}d^3x \quad (10)$$

It should be noted that the moment of inertia cannot be calculated directly as an integral quantity over the source of gravitational field (Stergioulas 2003). In addition, there exists no unique generalization of the Newtonian definition of the moment of inertia in General Relativity and therefore  $I = J/\Omega$  is a natural choice for calculating this important quantity.

For rotational frequencies much lower than the Kepler frequency (the highest possible rotational rate supported by a given EOS), i.e.  $\nu/\nu_k \ll 1$  ( $\nu = \Omega/(2\pi)$ ), the deviations from spherical symmetry are very small, so that the moment of inertia can be approximated from spherical stellar models. In what follows we review briefly this slow-rotation approximation, see e.g. (Hartle 1967). In the slow-rotational limit the metric can be written in spherical coordinates as (in geometrized units  $G = c = 1$ )

$$ds^2 = -e^{2\phi(r)}dt^2 + \left(1 - \frac{2m(r)}{r}\right)^{-1} dr^2 - 2\omega r^2 \sin^2 \theta dt d\phi + r^2(d\theta^2 + \sin^2 \theta d\phi^2) \quad (11)$$

---

<sup>1</sup>Thanks to Nikolaos Stergioulas the *RNS* code is available as a public domain program at <http://www.gravity.phys.uwm.edu/rns/>

In the above equation  $m(r)$  is the total gravitational mass within radius  $r$  satisfying the usual equation

$$\frac{dm(r)}{dr} = 4\pi\epsilon(r)r^2 \quad (12)$$

and  $\omega(r) \equiv (d\phi/dt)_{ZAMO}$  is the Lense-Thirring angular velocity of a zero-angular-momentum observer (ZAMO). Up to first order in  $\omega$  all metric functions remain spherically symmetric and depend only on  $r$  (Morrison et al. 2004). In the stellar interior the Einstein's field equations reduce to

$$\frac{d\phi(r)}{dr} = m(r) \left[ 1 + \frac{4\pi r^3 P(r)}{m(r)} \right] \left[ 1 - \frac{2m(r)}{r} \right]^{-1} \quad (r < R_{star}) \quad (13)$$

and

$$\frac{1}{r^3} \frac{d}{dr} \left( r^4 j(r) \frac{d\bar{\omega}(r)}{dr} \right) + 4 \frac{dj(r)}{dr} \bar{\omega}(r) = 0 \quad (r < R_{star}), \quad (14)$$

with  $\bar{\omega} \equiv \Omega - \omega$  the dragging angular velocity (the angular velocity of the star relative to a local inertial frame rotating at  $\omega$ ) and

$$j \equiv \left( 1 - \frac{2m(r)}{r} \right)^{1/2} e^{-\phi(r)} \quad (15)$$

Outside the star the metric functions become

$$e^{2\phi} = \left( 1 - \frac{2M}{r} \right) \quad (r > R_{star}) \quad (16)$$

and

$$\omega = \frac{2J}{r^3} \quad (r > R_{star}), \quad (17)$$

where  $M = m(r = R) = 4\pi \int_0^R \epsilon(r') r'^2 dr'$  is the total gravitational mass and  $R$  is the stellar radius defined as the radius at which the pressure drops to zero ( $P(r = R) = 0$ ). At the star's surface the interior and exterior solutions are matched by satisfying the appropriate boundary conditions

$$\bar{\omega}(R) = \Omega - \frac{R}{3} \left( \frac{d\bar{\omega}}{dr} \right)_{r=R} \quad (18)$$

and

$$\phi(r) = \frac{1}{2} \ln \left( 1 - \frac{2M}{r} \right) \quad (19)$$

The moment of inertia  $I = J/\Omega$  then can be computed from Eq. (10). With  $\Omega = u^\phi/u^t$  and retaining only first order terms in  $\omega$  and  $\Omega$ , the moment of inertia reads (Morrison et al. 2004; Lattimer & Prakash 2000)

$$I \approx \frac{8\pi}{3} \int_0^R (\epsilon + P) e^{-\phi(r)} \left[ 1 - \frac{2m(r)}{r} \right]^{-1} \frac{\bar{\omega}}{\Omega} r^4 dr \quad (20)$$

This slow-rotation approximation for the neutron-star moment of inertia neglects deviations from spherical symmetry and is independent of the angular velocity  $\Omega$  (Morrison et al. 2004). For neutron stars with masses greater than  $1M_{\odot}$  Lattimer & Schutz (2005) found that, for slow-rotations, the momenta of inertia computed through the above formalism (Eq. (20)) can be approximated very well by the following empirical relation:

$$I \approx (0.237 \pm 0.008)MR^2 \left[ 1 + 4.2 \frac{Mkm}{M_{\odot}R} + 90 \left( \frac{Mkm}{M_{\odot}R} \right)^4 \right] \quad (21)$$

The above equation is shown (Lattimer & Schutz 2005) to hold for a wide class of EOSs except for ones with appreciable degree of softening, usually indicated by achieving a maximum mass of  $\sim 1.6M_{\odot}$  or less. Since none of the EOSs employed in this paper exhibit such pronounced softening, Eq. (21) is a good approximation for the momenta of inertia of *slowly* rotating stars.

#### 4. Results and discussion

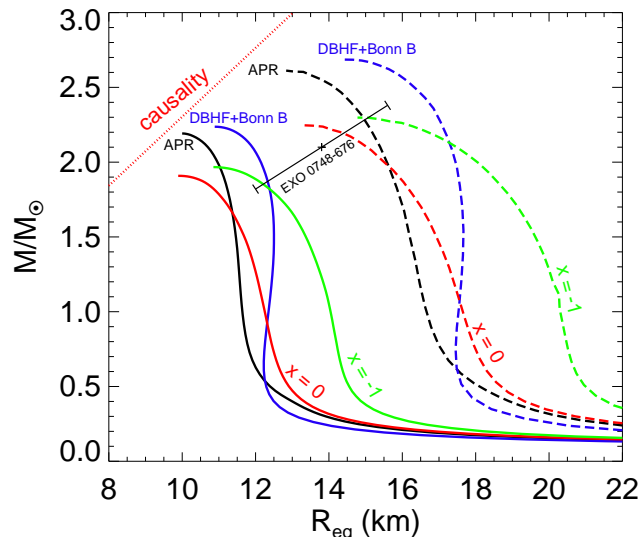


Fig. 3.— (Color online) Mass-radius relation for static and maximally rotating neutron stars. Solid lines correspond to static and broken lines to maximally rotating stellar models. Taken from (Krastev et al. 2008).

We calculate the neutron star moment of inertia applying several nucleonic EOSs (see Section 2) considering both slow- and rapid-rotation regimes. In Fig. 3 we show stellar sequences computed with the *RNS* code for spherical and maximally rotating models. As seen

in the figure, rapid rotation alters significantly the mass-radius relation of rapidly rotating stars (with respect to static configurations). Generally, for a given EOS it increases the maximum possible mass by  $\sim 15\%$ , while reducing/increasing the polar/circumferential radius by several kilometers, leading to an overall oblate shape of the rotating star. The degree to which the neutron star properties are impacted by rapid rotation depends on the details of the EOS: it is greater for models from stiffer EOS which produce less centrally condensed and gravitational bound neutron stars (Friedman et al. 1984). In view of these considerations, one should expect similar changes in the moment of inertia of rapidly rotating neutron stars (with respect to static models). We address these and other implications next.

#### 4.1. Slow rotation

If the rotational frequency is much smaller than the Kepler frequency, the deviations from spherical symmetry are negligible and the moment of inertia can be calculated applying the slow-rotation approximation discussed briefly in Section 3. For this case Lattimer & Schutz (2005) showed that the moment of inertia can be very well approximated by Eq. (21). In Fig. 4 we display the moment of inertia as a function of stellar mass for slowly rotating neutron stars as computed with the empirical relation (21). As shown in Fig. 3, above  $\sim 1.0M_{\odot}$  the neutron star radius remains approximately constant before reaching the maximum mass

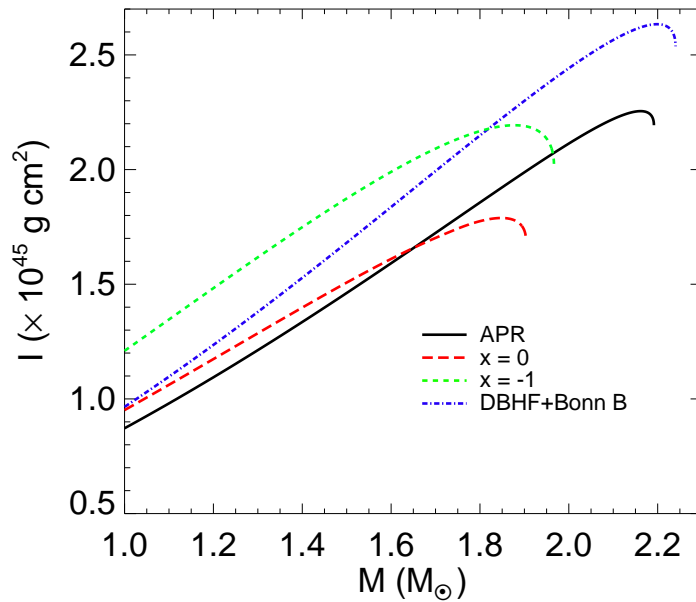


Fig. 4.— (Color online) Total moment of inertia of neutron stars estimated with Eq. (21).

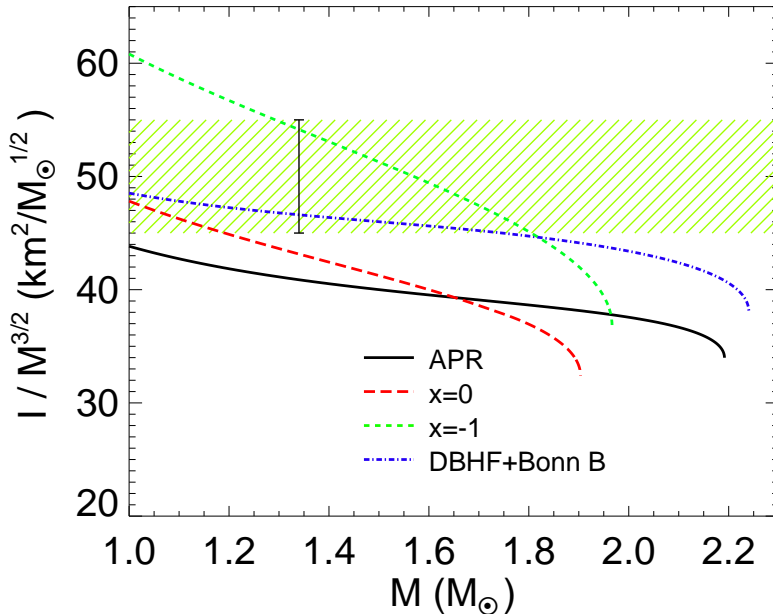


Fig. 5.— (Color online) The moment of inertia scaled by  $M^{3/2}$  as a function of the stellar mass  $M$ . The shaded band illustrates a 10% error of hypothetical  $I/M^{3/2}$  measurement of  $50 \text{ km}^2 M_{\odot}^{-1/2}$ . The error bar shows the specific case in which the mass is  $1.34M_{\odot}$  (after (Lattimer & Schutz 2005)).

supported by a given EOS. The moment of inertia ( $I \sim MR^2$ ) thus increases almost linearly with stellar mass for all models. Right before the maximum mass is achieved, the neutron star radius starts to decrease (Fig. 3), which causes the sharp drop in the moment of inertia observed in Fig. 4. Since  $I$  is proportional to the mass and the square of the radius, it is more sensitive to the density dependence of the nuclear symmetry energy, which determines the neutron star radius. Here we recall that the  $x = -1$  EOS has much stiffer symmetry energy (with respect to the one of the  $x = 0$  EOS), which results in neutron star models with larger radii and, in turn, momenta of inertia. For instance, for a “canonical” neutron star ( $M = 1.4M_{\odot}$ ), the difference in the moment of inertia is more than 30% with the  $x = 0$  and the  $x = -1$  EOSs. In Fig. 5 we take another view of the moment of inertia where  $I$  is scaled by  $M^{3/2}$  as a function of the stellar mass (after (Lattimer & Schutz 2005)).

The discovery of the extremely relativistic binary pulsar PSR J0737-3039A,B provides an unprecedented opportunity to test General Relativity and physics of pulsars (Burgay et al. 2003). Lattimer & Schutz (2005) estimated that the moment of inertia of the A component of the system should be measurable with an accuracy of about 10%. Given that the masses of both stars are already accurately determined by observations, a measurement of the moment

Table 3: Numerical results for PSR J0737-3039A ( $M_A = 1.338M_\odot$ ,  $\nu_A = 44.05Hz$ ).

EOS	$\epsilon_c(\times 10^{14}g\ cm^{-3})$	$R_{eq}(km)$	$I(\times 10^{45}g\ cm^2)$	$I^{LS}(\times 10^{45}g\ cm^2)$
MDI(x=-1)	7.04	13.75 (13.64)	1.63	1.67
DBHF+Bonn B	7.34	12.56 (12.47)	1.57	1.43
MDI(x=0)	9.85	12.00 (11.90)	1.30	1.34
APR	9.58	11.60 (11.52)	1.25	1.26

The first column identifies the equation of state. The remaining columns exhibit the following quantities: central mass-energy density, equatorial radius (the numbers in the parenthesis are the radii of the spherical models; the deviations from sphericity due to rotation are  $\sim 1\%$ ), total moment of inertia, total moment of inertia  $I^{LS}$  as computed with Eq. (21).

of inertia of even one neutron star could have enormous importance for the neutron star physics (Lattimer & Schutz 2005). (The significance of such a measurement is illustrated in Fig. 5. As pointed by Lattimer & Schutz (2005), it is clear that very few EOSs would survive these constraints.) Thus, theoretical predictions of the moment of inertia are very timely. Calculations of the moment of inertia of pulsar A ( $M_A = 1.338M_\odot$ ,  $\nu_A = 44.05Hz$ ) have been reported by Morrison et al. (2004) and Bejger et al. (2005). In Table 3 we show the moment of inertia and (other selected quantities) of PSR J0737-3039A computed with the *RNS* code using the EOSs employed in this study. Our results with the APR EOS are in very good agreement with those by Morrison et al. (2004) ( $I^{APR} = 1.24 \times 10^{45}g\ cm^2$ ) and Bejger et al. (2005) ( $I^{APR} = 1.23 \times 10^{45}g\ cm^2$ ). In the last column of Table 3 we also include results computed with the empirical relation (Eq. (21)). From a comparison with the results from the exact numerical calculation we conclude that Eq. (21) is an excellent approximation for the moment of inertia of slowly-rotating neutron stars. (The average uncertainty of Eq. (21) is  $\sim 2\%$ , except for the DBHF+BonnB EOS for which it is  $\sim 8\%$ .) Our results (with the MDI EOS) allowed us to constrain the moment of inertia of pulsar A to be in the range  $I = (1.30 - 1.63) \times 10^{45}(g\ cm^2)$ .

## 4.2. Rapid rotation

In this subsection we turn our attention to the moment of inertia of rapidly rotating neutron stars. In Fig. 6 we show the moment of inertia as a function of stellar mass for neutron star models spinning at the mass-shedding (Kepler) frequency. The numerical calculation is performed with the *RNS* code. We observe that the momenta of inertia of rapidly rotating neutron stars are significantly larger than those of slowly rotating models (for a fixed mass).

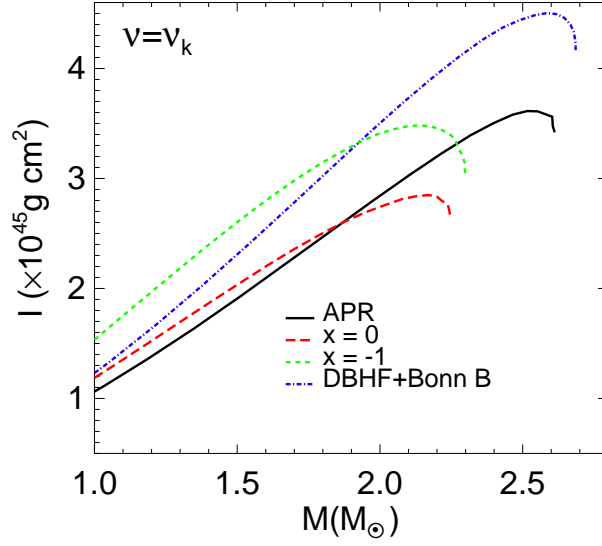


Fig. 6.— (Color online) Total moment of inertia for Keplerian models. The neutron star sequences are computed with the *RNS* code.

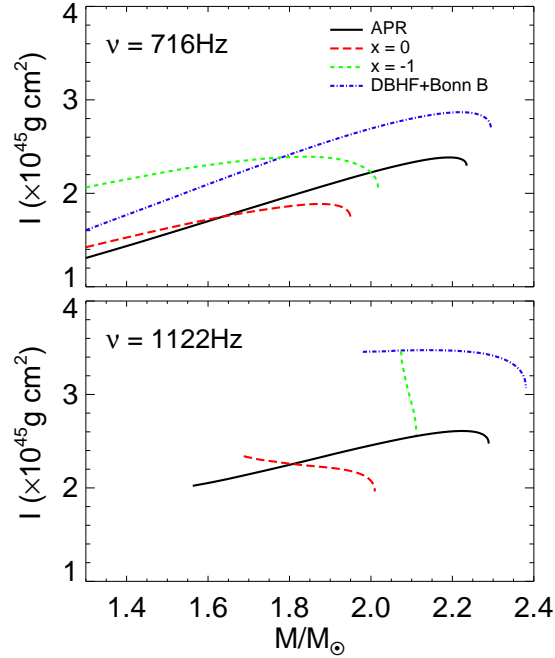


Fig. 7.— (Color online) Total moment of inertia as a function of stellar mass for models rotating at 716 Hz (upper frame) and 1122 Hz (lower frame).

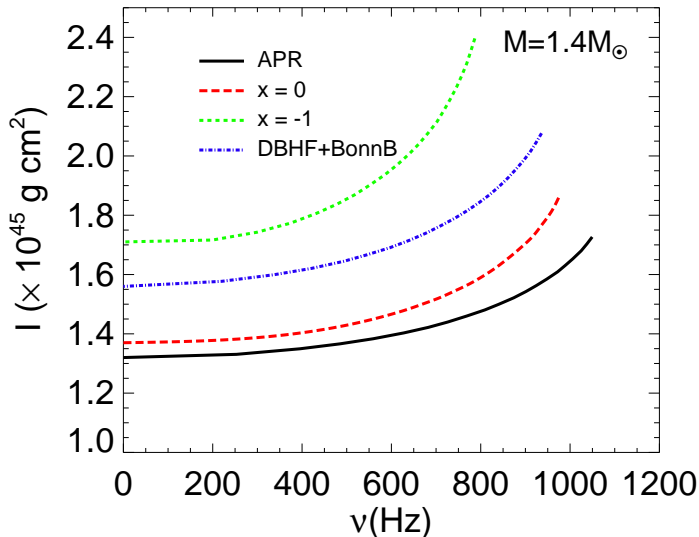


Fig. 8.— (Color online) Total moment of inertia as a function of rotational frequency for stellar models with mass  $M = 1.4M_{\odot}$ .

This is easily understood in terms of the increased (equatorial) radius (Fig. 3).

We also compute the momenta of inertia of neutron stars rotating at 716 (Hessels et al. 2006) and 1122Hz (Kaaret et al. 2007) which are the rotational frequencies of the fastest pulsars of today. The numerical results are presented in Fig. 7. As demonstrated by Bejger et al. (2007) and most recently by Krastev et al. (2008), the range of the allowed masses supported by a given EOS for rapidly rotating neutron stars becomes narrower than the one for static configurations. The effect becomes stronger with increasing frequency and depends upon the EOS. This is also illustrated in Fig. 7, particularly in the lower panel. Additionally, the moment of inertia shows increase with rotational frequency at a rate dependent upon the details of the EOS. This is best seen in Fig. 8 where we display the moment of inertia as a function of the rotational frequency for stellar models with a fixed mass ( $M = 1.4M_{\odot}$ ). The neutron star sequences shown in Fig. 8 are terminated at the mass-shedding frequency. At the lowest frequencies the moment of inertia remains roughly constant for all EOSs (which justifies the application of the slow-rotation approximation and Eq. (21)). As the stellar models approach the Kepler frequency, the moment of inertia exhibits a sharp rise. This is attributed to the large increase of the circumferential radius as the star approaches the “mass-shedding point”. As pointed by Friedman et al. (1984), properties of rapidly rotating neutron stars display greater deviations from those of spherically symmetric (static) stars for models computed with stiffer EOSs. This is because such models are less centrally condensed and gravitationally bound. This also explains why the momenta of inertia of rapidly

rotating neutron star configurations from the  $x = -1$  EOS show the greatest deviation from those of static models.

### 4.3. Fractional moment of inertia of the neutron star crust

As it was discussed extensively by Lattimer & Prakash (2000) (and others), the neutron star crust thickness might be measurable from observations of pulsar glitches, the occasional disrupts of the otherwise extremely regular pulsation from magnetized, rotating neutron stars. The canonical model of Link et al. (1999) suggests that glitches are due to the angular momentum transfer from superfluid neutrons to normal matter in the neutron star crust, the region of the star containing nuclei and nucleons that have dripped out of nuclei. This region is bound by the neutron drip density at which nuclei merge into uniform nucleonic matter. Link et al. (1999) concluded from the observations of the Vela pulsar that at least 1.4% of the total moment of inertia resides in the crust of the Vela pulsar. For slowly rotating neutron stars, applying several realistic hadronic EOSs that permit maximum masses of at least  $\sim 1.6M_\odot$  Lattimer & Prakash (2000) found that the fractional moment of inertia,  $\Delta I/I$ , can be expressed approximately as

$$\frac{\Delta I}{I} \simeq \frac{28\pi P_t R^3}{3Mc^2} \frac{(1 - 1.67\beta - 0.6\beta^2)}{\beta} \left[ 1 + \frac{2P_t(1 + 5\beta - 14\beta^2)}{\rho_t m_b c^2 \beta^2} \right]^{-1} \quad (22)$$

In the above equation  $\Delta I$  is the moment of inertia of the neutron star crust,  $I$  is the total moment of inertia,  $\beta = GM/Rc^2$  is the compactness parameter,  $m_b$  is the average nucleon mass,  $\rho_t$  is the transition density at the crust-core boundary, and  $P_t$  is the transition pressure. The determination of the transition density itself is a very complicated problem. Different approaches often give quite different results. Similar to determining the critical density for the spinodal decomposition for the liquid-gas phase transition in nuclear matter, for uniform *npe*-matter, Lattimer & Prakash (2000) and more recently Kubis (2007) have evaluated the crust transition density by investigating when the incompressibility of *npe*-matter becomes negative, i.e

$$K_\mu = \rho^2 \frac{d^2 E_0}{d\rho^2} + 2\rho \frac{dE_0}{d\rho} + \delta^2 \left[ \rho^2 \frac{d^2 E_{sym}}{d\rho^2} + 2\rho \frac{dE_{sym}}{d\rho} - 2E_{sym}^{-1} \left( \rho \frac{dE_{sym}}{d\rho} \right)^2 \right] < 0 \quad (23)$$

(see Fig. 9) where  $E_0(\rho)$  is the EOS of symmetric nuclear matter,  $E_{sym}$  is the nuclear symmetry energy, and  $\delta = (\rho_n - \rho_p)/(\rho_n + \rho_p)$  is the asymmetry parameter. Using this approach and the MDI interaction, Kubis (2007) found the transition density of 0.119, 0.092, 0.095 and  $0.160 fm^{-3}$  for the  $x$  parameter of 1, 0,  $-1$  and  $-2$ , respectively. Similarly, we have calculated the transition densities and pressures for the EOSs employed in this work. Our

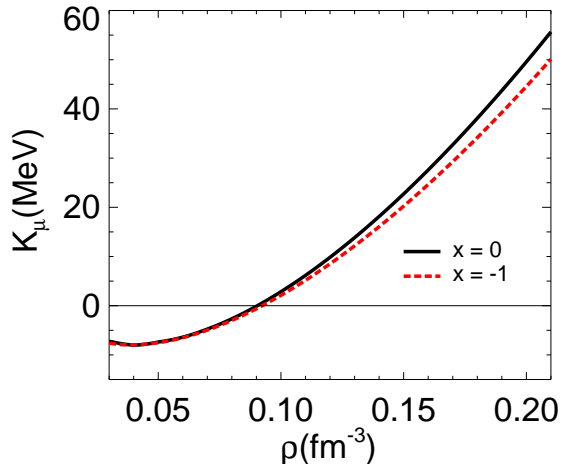


Fig. 9.— (Color online) The incompressibility,  $K_\mu$ , as a function of baryon density  $\rho$ .

results are summarized in Table 4. We find good agreement between our results and those by Kubis (2007) with the MDI interaction. It is interesting to notice that the transition densities predicted by all EOSs are in the same density range explored by heavy-ion reactions at intermediate energies. The MDI interaction with  $x = 0$  and  $x = -1$  constrained by the available data on isospin diffusion in heavy-ion reaction at intermediate energies thus limits the transition density rather tightly in the range of  $\rho_t = [0.091 - 0.093](fm^{-3})$ .

The fractional momenta of inertia  $\Delta I/I$  of the neutron star crusts are shown in Fig. 10 as computed through Eq. (22) with the parameters listed in Table 4. It is seen that the condition  $\Delta I/I > 0.014$  extracted from studying the glitches of the Vela pulsar does put a strict lower limit on the radius for a given EOS. It also limits the maximum mass to be less than about  $2M_\odot$  for all of the EOSs considered. Similar to the total momenta of inertia the ratio  $\Delta I/I$  changes more sensitively with the radius as the EOS is varied.

Table 4: Transition densities and pressures for the EOSs used in this paper.

EOS	MDI( $x=0$ )	MDI( $x=-1$ )	APR	DBHF+Bonn B
$\rho_t(fm^{-3})$	0.091 (0.095)	0.093 (0.092)	0.087	0.100
$P_t(MeV fm^{-3})$	0.645	0.982	0.513	0.393

The first row identifies the equation of state. The remaining rows exhibit the following quantities: transition density, transition pressure. The numbers in the parenthesis are the transition densities calculated by Kubis (2007).

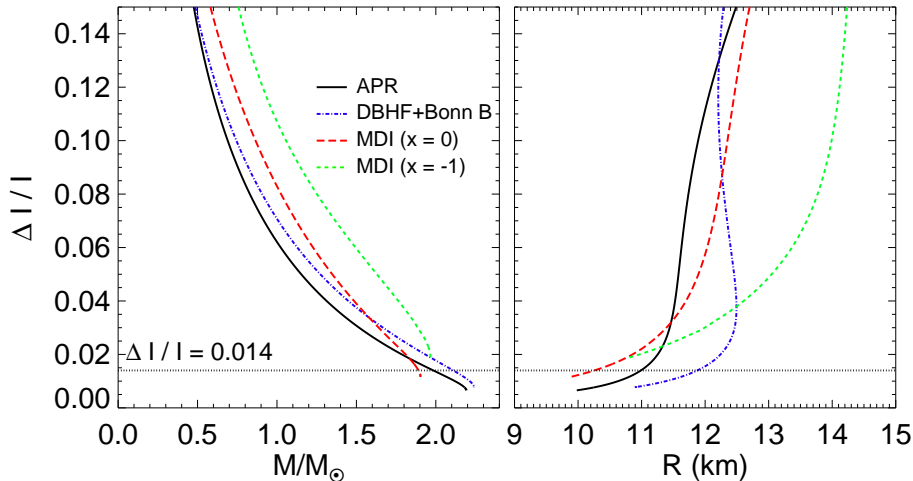


Fig. 10.— (Color online) The fractional moment of inertia of the neutron star crust as a function of the neutron star mass (left panel) and radius (right panel) estimated with Eq. (22). The constraint from the glitches of the Vela pulsar is also shown.

## 5. Summary

Recent experiments in terrestrial nuclear laboratories have narrowed down significantly the range of the EOS of neutron-rich nuclear matter although there are still many remaining challenges and uncertainties. In particular, the EOS for symmetric nuclear matter was constrained up to about five times the normal nuclear matter density by collective flow and particle production in relativistic heavy-ion reactions. The density dependence of the symmetry energy was constrained at subsaturation densities by isospin diffusion and isoscaling in heavy-ion reactions at intermediate energies. Applying the EOSs constrained by the heavy-ion reaction data we have studied the neutron star momenta of inertia of both slowly and rapidly rotating models within well established formalisms. We found that the moment of inertia of PSR J0737-3039A is limited in the range of  $I = (1.30 - 1.63) \times 10^{45} (g \text{ cm}^2)$ . The neutron star crust-core transition density falls in a very narrow interval of  $\rho_t = [0.091 - 0.093] (fm^{-3})$ . The corresponding fractional momenta of inertia  $\Delta I/I$  of the neutron star crust are also constrained. It is also found that the moment of inertia increases with rotational frequency at a rate strongly dependent upon the EOS used.

## Acknowledgements

We would like to thank Lie-Wen Chen, Wei-Zhou Jiang and Jun Xu for helpful discussions. Plamen Krastev acknowledges the hospitality of the Institute for Nuclear Theory (INT) at the University of Washington where parts of this work were accomplished. This work was supported by the National Science Foundation under Grant No. PHY0652548 and the Research Corporation under Award No. 7123.

## REFERENCES

- Akmal, A., Pandharipande, V. R., & Ravenhall, D. G. 1998, Phys. Rev., C58, 1804
- Alonso, D. & Sammarruca, F. 2003, Phys. Rev., C67, 054301
- Ansorg, M., Kleinwächter, A., & Meinel, R. 2002, A&A, 381, L49
- Baran, V., Colonna, M., Greco, V., & Di Toro, M. 2005, Phys. Rept., 410, 335
- Basu, D.N., Chowdhury, P.R., Samanta, C., 2006, Acta Phys. Polon. B37, 2869; Basu, D.N. and Mukhopadhyay, T., 2007, *ibid*, B38, 169; Mukhopadhyay T. and Basu, D.N., 2007, *ibid*, B38, 3225
- Bertsch, G.F., and Das Gupta, S., 2005, Phys. Rept., 160, 189
- Bejger, M., Bulik, T., & Haensel, P. 2005, MNRAS, 364, 635
- Bejger, M., Haensel, P., & Zdunik, J. L. 2007, A&A, 464, L49
- Bombaci, I., Thampan, A. V., & Datta, B. 2000, Astrophys. J., 541, L71
- Bonazzola, S., Gourgoulhon, E., & Marck, J.-A. 1998, Phys. Rev. D, 58, 104020
- Bonazzola, S., Gourgoulhon, E., Salgado, M., & Marck, J. A. 1993, A&A, 278, 421
- Brown, B.A., 2000, Phys. Rev. Lett. 85, 5296
- Burgay, M., D’Amico, N., Possenti, A., Manchester, R. N., Lyne, A. G., Joshi, B. C., McLaughlin, M. A., Kramer, M., Sarkissian, J. M., Camilo, F., Kalogera, V., Kim, C., & Lorimer, D. R. 2003, Nature, 426, 531
- Chabanat. E., et al., 1997, Nucl. Phys. A 627, 710; 1998, *ibid*, 635, 231
- Chen, L. W., Ko, C. M., & Li, B.-A. 2005, Phys. Rev. Lett., 94, 032701

- Chen, L. W., Ko, C. M., & Li, B.-A. 2005, *Phys. Rev.* C72, 064309
- Chen, L. W., Ko, C. M., Li, B. A., Yong, G. C., 2007, *Frontiers of Physics in China* 2, 327
- Cook, G. B., Shapiro, S. L., & Teukolsky, S. A. 1994, *ApJ*, 424, 823
- Danielewicz, P., Lacey, R., & Lynch, W. G. 2002, *Science*, 298, 1592
- Das, C. B., Gupta, S. D., Gale, C., & Li, B.-A. 2003, *Phys. Rev.*, C67, 034611
- Dieperink, A.E.L., Dewulf, Y., Van Neck, D., Waroquier, M., Rodin, V., 2003, *Phys. Rev. C* 68, 064307
- Friedman, J. L., Parker, L., & Ipser, J. R. 1984, *Nature*, 312, 25
- Friedman, J. L., Parker, L., & Ipser, J. R. 1986, *Astrophys. J.*, 304, 115
- Furnstahl, R.J., 2002, *Nucl. Phys. A* 706, 85
- Haensel, P. & Pichon, B. 1994, *Astron. Astrophys.*, 283, 313
- Hartle, J. B. 1967, *Astrophys. J.*, 150, 1005
- Hartle, J. B. & Thorne, K. S. 1968, *Astrophys. J.*, 153, 807
- Heiselberg, H. & Hjorth-Jensen, M. 2000, *Phys. Rept.*, 328, 237
- Heiselberg, H. & Pandharipande, V. 2000, *Ann. Rev. Nucl. Part. Sci.*, 50, 481
- Hessels, J. W. T., Ransom, S. M., Stairs, I. H., et al. 2006, *Science*, 311, 1901
- Horowitz, C. J., Pollock, S. J., Souder, P. A., and Michaels, R. 2001, *Phys. Rev.*, C63, 025501
- Horowitz, C. J. & Piekarewicz, J. 2001, *Phys. Rev. Lett.*, 86, 5647
- Horowitz, C. J. & Piekarewicz, J. 2002, *Phys. Rev.*, C66, 055803
- Jofre, P., Reisenegger, A., & Fernandez, R. 2006, *Phys. Rev. Lett.*, 97, 131102
- Kaaret, P., Prieskorn, J., in't Zand, J. J. M., et al. 2007, *Astrophys. J.*, 657, L97
- Khoa, D. T., Von Oertzen, W., & Ogloblin, A. A. 1996, *Nucl. Phys.*, A602, 98
- Komatsu, H., Eriguchi, Y., & Hachisu, I. 1989, *MNRAS*, 237, 355
- Krastev, P. G. & Sammarruca, F. 2006, *Phys. Rev.*, C74, 025808

- Krastev, P. G. & Li, B.-A. 2007, Phys. Rev. C76, 055804
- Krastev, P. G., Li, B.-A. & Worley, A. 2008, Astrophys. J., in press (0709.3621)
- Kubis, S. 2007, Phys. Rev., C76, 025801
- Kutschera, M., 1994, Phys. Lett. B340, 1; 1994, Z. Phys. A348, 263; 1989, Phys. Lett. B223, 11; 1993, Phys. Rev. C47, 1077
- Kutschera, M., Niemiec, J., 2000, Phys. Rev. C62, 025802
- Lattimer, J. M. & Prakash, M. 2007, Phys. Rept. 442, 109
- Lattimer, J. M., Schutz, B. F. 2005, Astrophys. J., 629, 979
- Lattimer, J. M. & Prakash, M. 2000, Phys. Rept., 333, 121
- Lattimer, J. M. & Prakash, M. 2004, Science, 304, 536
- Lattimer, J. M., Prakash, M., Masak, D., & Yahil, A. 1990, ApJ, 355, 241
- Li, B.-A. 2000, Phys. Rev. Lett., 85, 4221
- Li, B.-A. 2002, Phys. Rev. Lett., 88, 192701
- Li, B.-A. & Chen, L.-W. 2005, Phys. Rev., C72, 064611
- Li, B.-A., Ko, C. M., & Bauer, W. 1998, Int. J. Mod. Phys., E7, 147
- Li, B.-A., Ko, C.M., 1997, Nucl. Phys. A618, 498
- Li, B.-A., Ko, C. M., & Ren, Z.-Z. 1997, Phys. Rev. Lett., 78, 1644
- Li, B.-A., Das, C.B., Das Gupta, S., Gale, C., 2004, Phys. Rev. C69, 011603 (R); 2004, Nucl. Phys. A735, 563
- Li, B.-A., Yong, G. C., & Zuo, W. 2005, Phys. Rev. C71, 014608
- Li, B.-A. & Steiner, A. W. 2006, Phys. Lett., B642, 436
- Li, B.-A. & Udo Schroeder, W. 2001, Isospin Physics in Heavy-Ion Collisions at Intermediate Energies (New York: Nova Science)
- Link, B., Epstein, R.I. & Lattimer, J.M. 1999, Phys. Rev. Lett., 83, 3362
- Machleidt, R. 1989 Adv. Nucl. Phys., 19, 189

- Morrison, I. A., Baumgarte, T. W., Shapiro, S. L., & Pandharipande, V. R. 2004, *Astrophys. J.*, 617, L135
- Muller, H., Serot, B., 1995, *Phys. Rev. C*52, 2072
- Pandharipande, V.R., Garde, V.K., 1972, *Phys. Lett.* B39, 608
- Pethick, C. J., Ravenhall, D. G., & Lorenz, C. P. 1995, *Nucl. Phys.*, A584, 675
- Piekraewicz, J., 2007, *Phys. Rev. C*76, 064310.
- Prakash, M., Ainsworth, T.L., Lattimer, J.M., 1988, *Phys. Rev. Lett.* 61, 2518
- Prakash, M., Lattimer, J. M., Sawyer, R. F., & Volkas, R. R. 2001, *Ann. Rev. Nucl. Part. Sci.*, 51, 295
- Prakash, M., Prakash, M., Lattimer, J. M., & Pethick, C. J. 1992, *ApJ*, 390, L77
- Shetty, D., Yennello, S.J. and Souliotis, G.A., 2007, *Phys. Rev. C*75, 034602
- Shi, L. & Danielewicz, P. 2003, *Phys. Rev.*, C68, 064604
- Steiner, A. W. & Li, B.-A. 2005, *Phys. Rev.*, C72, 041601
- Steiner, A. W., Prakash, M., Lattimer, J. M., & Ellis, P. J. 2005, *Phys. Rept.*, 411, 325
- Stergioulas, N. 2003, *Living Rev. Rel.*, 6, 3
- Stergioulas, N. & Friedman, J. L. 1995, *Astrophys. J.*, 444, 306
- Stergioulas, N. & Friedman, J. L. 1998, *Astrophys. J.*, 492, 301
- Stone, J.R., Miller, J.C., Konciewicz, R., Stevenson, P.D., Strayer, M.R., 2003, *Phys. Rev. C*68, 034324
- Todd-Rutel, B. G. & Piekarewicz, J. 2005, *Phys. Rev. Lett.*, 95, 122501
- Tsang, M.B. et al., 2001, *Phys. Rev. Lett.* 86, 5023
- Tsang, M.B. et al., 2004, *Phys. Rev. Lett.* 92, 062701
- Weber, F. 1999, *Pulsars as Astrophysical Laboratories for Nuclear and Particle Physics* (Bristol, Great Britan: IOP Publishing)
- Wiringa, R.B., 1988, *Phys. Rev. C*38, 2967

Wiringa, R.B., Fiks, V., Fabrocini, A., 1988, Phys. Rev. C 38, 1010

Yakovlev, D. G. & Pethick, C. J. 2004, Ann. Rev. Astron. Astrophys., 42, 169